

UCSF

UC San Francisco Previously Published Works

Title

Exact, convergent periodic-orbit expansions of individual energy eigenvalues of regular quantum graphs.

Permalink

<https://escholarship.org/uc/item/0qg3s84h>

Journal

Physical review. E, Statistical, nonlinear, and soft matter physics, 65(4 Pt 2A)

ISSN

1539-3755

Authors

Blümel, R
Dabaghian, Y
Jensen, R V

Publication Date

2002-04-01

DOI

10.1103/PhysRevE.65.046222

Peer reviewed

Exact, convergent periodic-orbit expansions of individual energy eigenvalues of regular quantum graphs

R. Blümel, Y. Dabaghian, and R. V. Jensen

Department of Physics, Wesleyan University, Middletown, Connecticut 06459-0155

(Received 16 October 2001; published 8 April 2002)

We present exact, explicit, convergent periodic-orbit expansions for individual energy levels of regular quantum graphs in the paper. One simple application is the energy levels of a particle in a piecewise constant potential. Since the classical ray trajectories (including ray splitting) in such systems are strongly chaotic, this result provides an explicit quantization of a classically chaotic system.

DOI: 10.1103/PhysRevE.65.046222

PACS number(s): 05.45.Mt, 03.65.Sq

I. INTRODUCTION

Within the framework of semiclassical periodic-orbit theory the quantization procedures for integrable and chaotic systems differ substantially. An integrable system may be quantized using the Einstein-Brillouin-Keller theory [1]. The set of integrals

$$I_i = \int_{C_i} p_\mu dq^\mu = h(n_i + \mu_i), \quad i = 1, \dots, N, \quad (1)$$

extended along the N fundamental cycles C_i of the N -dimensional phase-space tori yield the (semiclassical) quantization conditions for every action variable I_i . Here the n_i 's are integer quantum numbers and the μ_i 's are Maslov indices. Although not exact in general, the quantization condition (1) does (implicitly) produce individual energy levels E_{n_1, \dots, n_N} that can be labeled, one by one, with the N quantum numbers n_1, \dots, n_N . This procedure differs markedly from the chaotic case where the focus is not on individual energy levels but on *global* characteristics of the spectrum. For instance, instead of finding individual energy levels as in Eq. (1), periodic-orbit quantization schemes for chaotic systems, such as, Gutzwiller's trace formula [1] compute the density of states

$$\rho(k) = \sum_{j=1}^{\infty} \delta(k - k_j), \quad (2)$$

from which individual energy levels are extracted indirectly as the singularities of ρ . In a chaotic system the only available classical input are the periodic orbits of the system and the density of states (2) is computed according to [1]

$$\rho(k) \approx \bar{\rho}(k) + \frac{1}{\pi} \text{Im} \sum_p T_p(E) \sum_{\nu=1}^{\infty} A_p^\nu(E) e^{i\nu S_p(E)}. \quad (3)$$

Here $\bar{\rho}(k)$ is the average density of states, $S_p(E)$, $T_p(E)$, and $A_p(E)$ are correspondingly the action, the period, and the weight factor of the prime periodic orbit labeled by p , and ν is the repetition index. Again, the scheme (3) is not usually exact. More seriously, however, in contrast to Eq. (1) it fails to produce individual energy levels in the form " $E_n = \dots$." The difference between Eq. (1) and Eq. (3) cannot be emphasized enough. While Eq. (1) allows us to "pick and

choose" a particular energy eigenvalue, in the chaotic case all of the eigenvalues have to be computed according to Eq. (3), and only a subsequent nonanalytic inspection and counting procedure allows us to focus on an individual energy level. There is, however, a class of quantum chaotic systems, regular quantum graphs [2], which are explicitly solvable analytically [2], i.e., exact periodic-orbit expansions of the form " $E_n = \dots$ " exist. The purpose of this paper is to expand considerably with respect to the work presented in [2] and to present a thorough discussion of our methods and their validity.

The organization of this paper is as follows. In Sec. II we extend the theory of quantum graphs [3–7] to include dressed graphs, i.e., quantum graphs with arbitrary potentials on their bonds. In Sec. III we define regular quantum graphs and present explicit, convergent periodic-orbit expansions of individual eigenvalues. These expansions are not just formal identities; the periodic-orbit expansions presented in Sec. III converge, and converge to the correct eigenvalues. In Sec. IV we present a worked example of a simple quantum graph whose spectrum is computed in three different ways: (i) numerically exactly, (ii) via the explicit periodic-orbit expansions presented in Sec. III, and (iii) via numerical integration using an exact trace formula for the density of states. The results of the three methods agree. This proves the validity and convergence of our approach. In Sec. V we summarize our results and conclude the paper.

II. DRESSED QUANTUM GRAPHS

A quantum graph consists of a quantum particle whose motion is confined to a one-dimensional network of N_B bonds B_{ij} connecting N_V vertices V_i . An example of a graph with six vertices and ten bonds is shown in Fig. 1. The topology of a given graph is fully characterized by its connectivity matrix C_{ij}

$$C_{ij} = C_{ji} = \begin{cases} 1 & \text{if } V_i \text{ and } V_j \text{ are connected} \\ 0 & \text{if they are not.} \end{cases} \quad (4)$$

Every bond B_{ij} , which connects the vertices V_i and V_j , supports a solution $\psi_{ij}(x)$ of the Schrödinger equation

$$\left(-i \frac{d}{dx} - A_{ij} \right)^2 \psi_{ij}(x) = E \psi_{ij}(x). \quad (5)$$

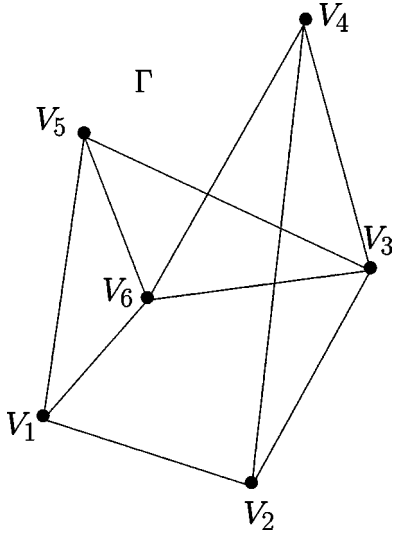


FIG. 1. A generic nonplanar graph with six vertices and ten bonds.

Here $0 \leq x \leq L_{ij}$ is the coordinate along B_{ij} measured from V_i to V_j , and $L_{ij} = L_{ji}$ is the length of the bond. A constant, real, skew symmetric matrix $A_{ij} = -A_{ji}$, which plays the role of a magnetic field vector potential, is sometimes introduced as a tool for braking the time-reversal symmetry, which, in turn, is known to affect the statistics of the level distribution [8,9].

In this paper we generalize the Schrödinger operator in Eq. (5) by adding potentials $U_{ij}(x, E)$ on the graph bonds. We call this generalization “dressing of the graph.” While, in general, the potentials $U_{ij}(x, E)$ may depend on the bond coordinate x and the energy E in an arbitrary way, we restrict ourselves here to the *scaling* case

$$U_{ij}(E) = \lambda_{ij}E, \quad \lambda_{ij} = \lambda_{ji}, \quad (6)$$

which allows us to introduce physical parallels between quantum graphs and ray-splitting systems [10–12]. A quantum graph with the potentials (6) on its bonds can also be viewed as a generalized step potential, such as, the one shown in Fig. 2(a). These potentials were studied earlier in great detail in connection with Anderson localization [13]. Potentials of this type can be represented by a linear graph, such as, the one shown in Fig. 2(b). Scaled potentials, such as Eq. (6) cast the Schrödinger equation into the form

$$\left(-i \frac{d}{dx} - A_{ij}\right)^2 \psi_{ij}(x) = \beta_{ij}^2 E \psi_{ij}(x), \quad (7)$$

where the parameters $\beta_{ij}^2 = 1 - \lambda_{ij}$, $\beta_{ij} = \beta_{ji}$ are defined on the corresponding bonds B_{ij} .

Depending on whether the energy $E = k^2$ of the particle is above or below the scaled potential height $U_{ij}(E)$, the solution of Eq. (7) on the bond B_{ij} is either a combination of the free waves

$$\psi_{ij}(x) = a_{ij} \frac{\exp[i(-\beta_{ij}k + A_{ij})x]}{\sqrt{\beta_{ij}k}} + b_{ij} \frac{\exp[i(\beta_{ij}k + A_{ij})x]}{\sqrt{\beta_{ij}k}},$$

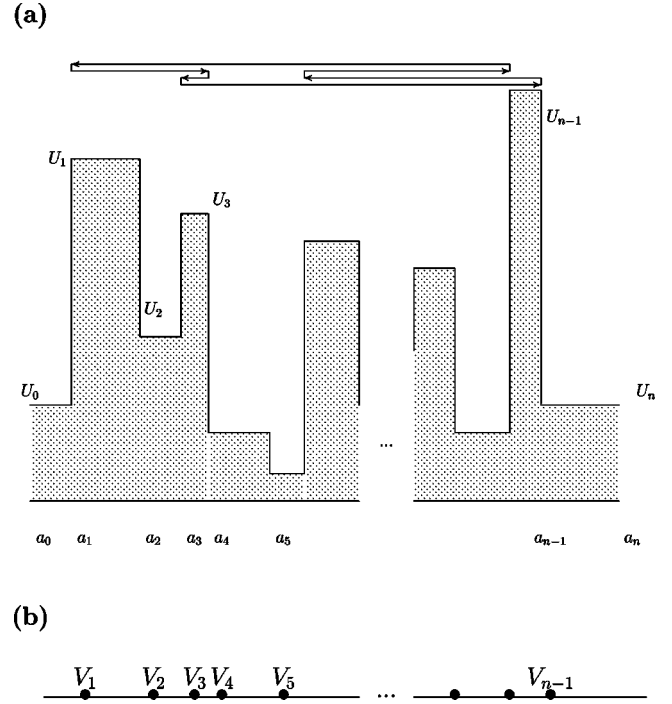


FIG. 2. An example of a (Manhattan) step potential (a) and its associated linear graph (b). Also shown is a non-Newtonian periodic orbit characterized by six above-barrier reflections.

$$\lambda_{ij} < 1, \quad (8)$$

or a combination of the tunneling solutions

$$\psi_{ij}(x) = a_{ij} \exp[(-\beta_{ij}k + iA_{ij})x] + b_{ij} \exp[(\beta_{ij}k + iA_{ij})x], \quad \lambda_{ij} > 1, \quad (9)$$

where the factors $(\beta_{ij}k)^{-1/2}$ in the propagating waves (8) were introduced to ensure proper flux normalization [14]. Due to the scaling assumption, there is no transition between these two cases as a function of E . From now on we shall assume that the energy E is kept above the maximal scaled potential height

$$\lambda_{ij} < 1, \quad i, j = 1, \dots, N_V, \quad C_{ij} \neq 0, \quad (10)$$

which will allow us to exclude the tunneling solutions (9). At every vertex V_i , the bond wave functions satisfy the continuity conditions

$$\psi_{ij}(x)|_{x=0} = \varphi_i C_{ij}, \quad i, j = 1, \dots, N_V \quad (11)$$

and the current conservation conditions

$$\sum_{j=1}^{N_V} C_{ij} \left(-i \frac{d}{dx} - A_{ij}\right) \psi_{ij}(x)|_{x=0} = -i \lambda_i \varphi_i, \quad i, j = 1, \dots, N_V. \quad (12)$$

Here φ_i is the value of the wave function at the vertex V_i , and the λ_i 's are free parameters of the problem for which the scaling is introduced as

$$\lambda_i = \lambda_i^0 k. \quad (13)$$

The conditions (11) and (12) are consistent only for a discrete set of wave numbers k_n , which defines the spectrum of the quantum graph problem. Since $\psi_{ij}(x)$ and $\psi_{ji}(y)$ represent the same wave function on the bond connecting the vertices V_i and V_j (the only difference is that x is measured from vertex V_i and y is measured from vertex V_j), we have

$$\psi_{ji}(L_{ij} - x) = \psi_{ij}(x). \quad (14)$$

Using Eq. (8) we obtain

$$\begin{aligned} \psi_{ji}(L_{ij} - x) &= a_{ji} \frac{\exp[i(-\beta_{ij}k + A_{ji})(L_{ij} - x)]}{\sqrt{\beta_{ij}k}} \\ &+ b_{ji} \frac{\exp[i(\beta_{ij}k + A_{ji})(L_{ij} - x)]}{\sqrt{\beta_{ij}k}} = \psi_{ij}(x). \end{aligned} \quad (15)$$

Therefore, the coefficients a_{ij} and b_{ij} are related according to

$$\begin{aligned} a_{ji} &= b_{ij} \exp[i(\beta_{ij}k + A_{ij})L_{ij}] \\ b_{ji} &= a_{ij} \exp[i(-\beta_{ij}k + A_{ij})L_{ij}]. \end{aligned} \quad (16)$$

The coefficients a_{ij} and a_{ji} , (b_{ij} and b_{ji}) are considered different. This implies that the bonds of the graph are directed. Equations (16) can be written in matrix form as

$$\vec{a} = P \tilde{D}(k) \vec{b}, \quad (17)$$

where \vec{a} and \vec{b} are the $2N_B$ -dimensional vectors of coefficients, \tilde{D} is a diagonal matrix in the $2N_B \times 2N_B$ space of directed bonds, and

$$P = \begin{pmatrix} 0 & 1_{N_B} \\ 1_{N_B} & 0 \end{pmatrix}, \quad (18)$$

where 1_{N_B} is the N_B -dimensional unit matrix. Explicitly we have

$$\tilde{D}_{ij,pq}(k) = \delta_{ip} \delta_{jq} \exp[i(\beta_{ij}k + A_{ij})L_{ij}]. \quad (19)$$

The pairs of indices (ij) , (pq) , identifying the bonds of the graph Γ , play the role of the indices of the matrix $\tilde{D}(k)$. Alternatively the wave function can be written as a linear combination of plane waves scattering off V_i . An incoming wave with normalized flux on the bond $B_{j'i}$ gives rise to a partial wave contribution scattering into bond B_{ij} according to

$$\begin{aligned} \psi_{jj'}^{(i)}(x_j) &= \delta_{jj'} \frac{\exp[i(-\beta_{ij}k + A_{ij})x_j]}{\sqrt{\beta_{ij}k}} \\ &+ \sigma_{j,j'}^{(i)} \frac{\exp[i(\beta_{ij}k + A_{ij})x_j]}{\sqrt{\beta_{ij}k}}. \end{aligned} \quad (20)$$

Here $\sigma_{j,j'}^{(i)}(k)$ is the matrix element of the vertex scattering matrix $\sigma^{(i)}(k)$, which distributes the incoming flux on bond $B_{j'i}$ into the bond B_{ij} . The wave function $\psi_{ij}(x_j)$ on the bond B_{ij} is a superposition of the partial waves (20) with amplitudes $a_{ij'}$, corresponding to the incoming flux on the bond $B_{j'i}$ towards the vertex V_i , i.e.,

$$\psi_{ij}(x_j) = \sum_{j'} a_{ij'} \psi_{jj'}^{(i)}(x_j). \quad (21)$$

Using the representation (8) of ψ_{ij} in Eq. (21) and comparing coefficients yields

$$b_{ij} = \sum_{j'} \sigma_{j,j'}^{(i)} a_{ij'}. \quad (22)$$

Substituting Eq. (20) into the boundary conditions, we obtain the vertex scattering matrix

$$\sigma_{j,j'}^{(i)} \equiv \sigma_{ji,ij'}^{(i)} = \left(-\delta_{jj'} + \frac{2\sqrt{\beta_{ij}\beta_{ij'}}}{v_i + i\lambda_i^0} \right) C_{ji} C_{ij'} \quad (23)$$

with

$$v_i = \sum_{j=1}^{N_V} \beta_{ij} C_{ij}. \quad (24)$$

We see that, in the scaling case, the matrix elements $\sigma_{j,j'}^{(i)}$ of the vertex scattering matrix $\sigma^{(i)}$ are k -independent constants. The matrix element $\sigma_{j,j}^{(i)}$ has the meaning of the reflection coefficient from the vertex V_i along the bond B_{ij} , and the elements $\sigma_{j,j'}^{(i)}$, $j \neq j'$ are the transmission coefficients for transitions between different bonds. Equation (22) can be written as

$$\vec{b} = \tilde{T} \vec{a}, \quad (25)$$

where

$$\tilde{T} \equiv \tilde{T}_{ij,nm} = \delta_{in} C_{ji} C_{nm} \sigma_{j,m}^{(i)}. \quad (26)$$

Equations (17) and (25) together result in

$$\vec{a} = S(k) \vec{a}, \quad (27)$$

where $S(k)$ (the total graph scattering matrix) is given by

$$S(k) = D(k) T \quad (28)$$

and $D = P \tilde{D} P$ and $T = P \tilde{T}$. The consistency of the system of linear Eqs. (27) requires the spectral equation

$$\Delta(k) = \det[1 - S(k)] = 0 \quad (29)$$

to be satisfied. This condition defines the set of allowed momenta $\{k_n\}$.

The density of the momentum states of the dressed quantum graph is given by

$$\rho(k) = \sum_{n=1}^{\infty} \delta(k - k_n), \quad (30)$$

where the k_n 's are the solutions of Eq. (29). An exact periodic-orbit expansion for $\rho(k)$ can be obtained directly from the spectral Eq. (29) as follows [3–7]. The logarithmic derivative of Eq. (29) is singular at each one of its roots. Between roots, the phase of the spectral determinant varies slowly such that

$$\rho(k) = \bar{\rho}(k) - \frac{1}{\pi} \lim_{\epsilon \rightarrow 0} \text{Im} \frac{d}{dk} \ln \det[1 - S(k + i\epsilon)]. \quad (31)$$

Using the well-known identity [3–7]

$$\ln \det[1 - S] = -\text{Tr} \sum_{n=1}^{\infty} \frac{1}{n} S^n, \quad (32)$$

we obtain

$$\rho(k) = \bar{\rho}(k) + \frac{1}{\pi} \lim_{\epsilon \rightarrow 0} \text{Im} \frac{d}{dk} \sum_{n=1}^{\infty} \frac{1}{n} \text{Tr}[S(k + i\epsilon)]^n. \quad (33)$$

Since the matrix indices of Eq. (28) correspond to the vertices of the graph, the trace of the n th power of the scattering matrix can be interpreted as a sum over all closed, connected sequences consisting of n bonds [3–7]. Classically, these periodic connected sequences of n bonds B_{ij} correspond to the periodic orbits traced by a point particle moving on the graph. Geometry and proliferation properties of the periodic orbits are determined completely by the topology of the graph.

The behavior of the periodic orbits on graphs exhibits the typical features of chaotic systems. The meaning of classical chaoticity on graphs is well defined, as demonstrated in the following. A classical graph system consists of a graph Γ and a point particle moving along its bonds, which scatters elastically at every vertex V_i along the direction of any of the bonds emanating from this particular vertex, with different probabilities. The probability amplitudes for every scattering channel can be obtained in the short wavelength limit from the quantum-mechanical transition amplitudes defined at every vertex V_i by the corresponding scattering matrix $\sigma_{j,j'}^{(i)}$. In the scaling case, the matrix elements $\sigma_{j,j'}^{(i)}$ are k -independent constants and thus do not depend on \hbar at all. Therefore, the same matrix elements determine both the quantum and the classical scattering probabilities.

For every given graph Γ the global average rate of exponential proliferation of periodic orbits, the topological entropy Λ , is given by

$$\Lambda = \lim_{l \rightarrow \infty} \frac{\ln[\mathcal{N}(l)]}{l}, \quad (34)$$

where l characterizes the length of the periodic orbits (for instance their code lengths) and $\mathcal{N}(l)$ is the total number of periodic orbits of length $\leq l$. The number of possible peri-

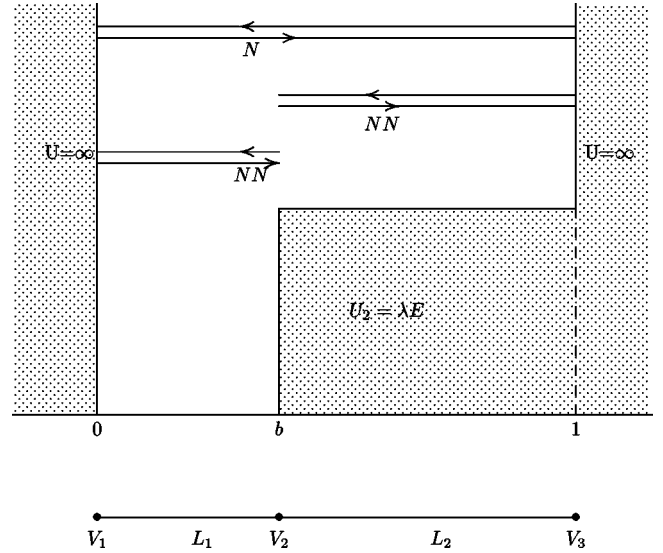


FIG. 3. A scaling step potential (top), equivalent to a three-vertex linear graph (bottom), as an example of a regular quantum graph. A Newtonian ($\mathcal{L}\mathcal{R}$) and two non-Newtonian (\mathcal{L}, \mathcal{R}) periodic orbits are also shown together with their $\mathcal{L}-\mathcal{R}$ codes.

odic orbits increases exponentially with their lengths (or, equivalently, the number of scattering events) with a rate Λ that depends only on the topology of the graph. Since the phase space of the system is bounded, the dynamics of such a particle is mixing [3].

Since we are focusing on the case $\lambda_{ij} < 1$, most of the classical periodic orbits on a graph are above-barrier reflection orbits as illustrated in Figs. 2 and 3. In the context of ray splitting these orbits are also known as non-Newtonian orbits [15–17]. The inclusion of all non-Newtonian orbits in our periodic-orbit expansions of individual eigenvalues discussed below is crucial for rendering these expansions exact.

Traversing the bond B_{ij} contributes the amount

$$S_{ij} = \int_{B_{ij}} (\beta_{ij} k + A_{ij}) dx \quad (35)$$

to the total action of the trajectory traced by the particle. These actions appear in the phases of the exact wave functions (8). This connection means that the semiclassical (eikonal) form is exact for the quantum graph wave functions. More importantly, the amplitudes $e^{iS_{ij}}$ determine the matrix $D(k)$, and hence the scattering matrix $S(k)$. As a consequence, the “closed bond sequence expansion” (33) can be written explicitly as a periodic-orbit expansion in terms of the phases (35)

$$\rho(k) = \bar{\rho}(k) + \frac{1}{\pi} \text{Re} \sum_p T_p(k) \sum_{\nu=1}^{\infty} \tilde{A}_p^\nu e^{i\nu \tilde{S}_p(k)}, \quad (36)$$

where \tilde{S}_p is the action of the prime periodic orbit p composed of the partial actions S_{ij} of Eq. (35) accumulated along the periodic orbit p , and $T_p(k) = d\tilde{S}_p(k)/dk$. The first term in Eq. (36) describes the average behavior of the density of states while the second represents the fluctuations around the

average. The amplitude of every periodic orbit p contains the constant factor $\exp(i\sum_{ij}A_{ij}L_{ij})$. This factor can be absorbed into the weight factor \tilde{A}_p . Thus, defining the reduced classical bond actions

$$S_{ij}^0 = \beta_{ij}L_{ij} \quad (37)$$

and the total reduced action S_p^0 accumulated along the periodic orbit p

$$S_p^0 = \sum_{ij \text{ along } p} S_{ij}^0, \quad (38)$$

the final periodic-orbit expansion for the density of states for scaling systems can be written as

$$\rho(k) = \bar{\rho}(k) + \frac{1}{\pi} \text{Re} \sum_p S_p^0 \sum_{\nu=1}^{\infty} A_p^\nu e^{i\nu S_p^0 k}. \quad (39)$$

In contrast with Eq. (3), the expression (39) for the density of states is exact; the action lengths S_p^0 and the weight factors A_p are k -independent constants.

The staircase function

$$N(k) = \sum_{n=1}^{\infty} \Theta(k - k_n) \quad (40)$$

is obtained by direct integration of Eq. (30). Using Eq. (39), $N(k)$ can be expanded as

$$\begin{aligned} N(k) &= \bar{N}(k) - \frac{1}{\pi} \lim_{\epsilon \rightarrow 0} \text{Im} \ln \det[1 - S(k + i\epsilon)] \\ &= \bar{N}(k) + \frac{1}{\pi} \text{Im} \sum_p \sum_{\nu=1}^{\infty} \frac{A_p^\nu}{\nu} e^{i\nu S_p^0 k}. \end{aligned} \quad (41)$$

Just like Eq. (39) this expansion is exact. The first term represents the average behavior of the staircase; the second term describes the fluctuations around the average.

III. REGULAR QUANTUM GRAPHS AND EXPLICIT SPECTRAL FORMULA

Since the scattering matrix (28) is a unitary matrix, its eigenvalues have the form $s_l = e^{i\theta_l(k)}$. Therefore, the spectral determinant (29) can be written as

$$\begin{aligned} \Delta(k) &= \prod_{l=1}^{2N_B} [1 - e^{i\theta_l(k)}] = \left[1 - \sum_{l=1}^{2N_B} e^{i\theta_l(k)} + \dots + e^{i\sum_{l=1}^{2N_B} \theta_l(k)} \right] \\ &= 2e^{i\Theta_0(k)} \left[\cos[\Theta_0(k)] + \sum_{j=1}^{N_C-1} (-1)^j \cos[\Theta_j(k)] \right], \end{aligned} \quad (42)$$

where

$$\Theta_0 = \frac{1}{2} \sum_{l=1}^{2N_B} \theta_l(k) \quad (43)$$

is the total phase of the spectral determinant, the Θ_j 's in Eq. (42) are linear combinations (sums and differences) of the phases $\theta_l(k)$ and $N_C = 4^{N_B}/2$. Evaluated directly, the spectral determinant is a polynomial of the (complex) matrix elements (19) with coefficients that are determined by the matrix elements (26). Factoring out the total phase (43) of this polynomial, we obtain the spectral equation in the form

$$\cos(S_0^0 k - \pi\gamma_0) = \Phi(k), \quad (44)$$

where

$$\Phi(k) = \sum_{i=1}^{N_\Gamma} a_i \cos(\Omega_i k - \pi\gamma_i). \quad (45)$$

Here, based on the reduced bond actions defined in Eq. (37), $S_0^0 = \sum_{ij} C_{ij} S_{ij}^0$ is the total reduced action length of the graph, the frequencies $\Omega_i < S_0^0$ are sums and differences of the reduced bond actions S_{ij}^0 and γ_0, γ_i are constants. For a general graph Γ it is difficult to calculate the precise number of cos terms N_Γ in Eq. (45). But an upper limit is given by the number of possible linear combinations of the N_B reduced bond actions S_{ij}^0 . Since there are

$$2^j \binom{N_B}{j}$$

ways of picking j actions out of N_B possible ones and combining them with “+” and “−” signs, we obtain

$$N_\Gamma \leq \sum_{j=1}^{N_B} 2^j \binom{N_B}{j} = -1 + \sum_{j=0}^{N_B} \binom{N_B}{j} 2^j 1^{N_B-j} = 3^{N_B} - 1. \quad (46)$$

A graph Γ is called *regular*, if the condition

$$\sum_{i=1}^{N_\Gamma} |a_i| = \alpha < 1 \quad (47)$$

is fulfilled. In case the condition (47) is satisfied, the spectral Eq. (44) can be immediately solved to yield the following implicit equation for the eigenvalues:

$$\begin{aligned} k_n &= \frac{\pi}{S_0^0} [n + \mu + \gamma_0] \\ &+ \frac{1}{S_0^0} \begin{cases} \arccos[\Phi(k_n)] & \text{for } n + \mu \text{ even} \\ \pi - \arccos[\Phi(k_n)] & \text{for } n + \mu \text{ odd,} \end{cases} \end{aligned} \quad (48)$$

where μ is a fixed integer, chosen such that k_1 is the first positive solution of Eq. (44). Equation (48) implies the existence of *separating points*

$$\hat{k}_n = \frac{\pi}{S_0^0} (n + \mu + \gamma_0 + 1) \quad (49)$$

in the spectrum k_n of Eq. (44). Because of Eq. (47) the points \hat{k}_n are never solutions of Eq. (48). They act as separators between k_n and k_{n+1} . Since the second term in Eq. (48) is bounded by π/S_0^0 , the deviation $|k_n - \hat{k}_n|$ never exceeds π/S_0^0 for any n . We emphasize, that the separators \hat{k}_n do not coincide with the average values \bar{k}_n of the roots k_n . The explicit decomposition of the roots k_n into an average part \bar{k}_n and a fluctuating part \tilde{k}_n , $k_n = \bar{k}_n + \tilde{k}_n$, can be obtained from the following equivalent formulation of Eq. (48):

$$k_n = \frac{\pi}{S_0^0} \left[n + \mu + \gamma_0 + \frac{1}{2} \right] + \frac{(-1)^{n+\mu}}{S_0^0} \left\{ \arccos[\Phi(k_n)] - \frac{\pi}{2} \right\}. \quad (50)$$

This form of k_n together with the boundedness of the second term in Eq. (50) proves rigorously that $\bar{N}(k)$, $\bar{\rho}(k)$ are of the form

$$\bar{N}(k) = \frac{S_0^0}{\pi} k + \bar{N}(0), \quad \bar{\rho}(k) = \frac{d\bar{N}(k)}{dk} = \frac{S_0^0}{\pi}. \quad (51)$$

Since $\Phi(k)$ contains only frequencies smaller than S_0^0 , every open interval $I_n = (\hat{k}_{n-1}, \hat{k}_n)$ contains one and only one root, i.e. k_n . Moreover, if Eq. (47) is fulfilled, the allowed zones $Z_n \subset I_n$, where the roots k_n can be found, narrows down to

$$k_n \in Z_n \equiv \left(\frac{\pi}{S_0^0} (n + \mu + \gamma_0 + u), \frac{\pi}{S_0^0} (n + \mu + \gamma_0 + 1 - u) \right), \quad (52)$$

where $u = \arccos(\alpha)/S_0^0$. Correspondingly, there exist forbidden regions R_n

$$R_n \equiv \left(\frac{\pi}{S_0^0} (n + \mu + \gamma_0 + 1 - u), \frac{\pi}{S_0^0} (n + \mu + \gamma_0 + 1 + u) \right), \quad (53)$$

where roots of Eq. (48) can never be found. Note that $\hat{k}_n \in R_n$. In the limit $\alpha \rightarrow 1$ ($u \rightarrow 0$), the width of the forbidden region R_n shrinks to zero, and the allowed zone Z_n occupies the whole root interval I_n .

The existence of the separating points (49) is the key to obtaining the explicit form of the periodic-orbit expansion for individual roots k_n . Multiplying both sides of Eq. (39) by k and integrating from \hat{k}_{n-1} to \hat{k}_n , we obtain

$$k_n = \hat{k}_n - \frac{\pi}{2S_0^0} - \frac{1}{\pi} \operatorname{Re} \sum_p \sum_{\nu=1}^{\infty} A_p^\nu \frac{e^{i\nu S_p^0 \hat{k}_n}}{\nu} \left\{ (1 - e^{-i\nu \omega_p}) \times \left(i\hat{k}_n - \frac{1}{\nu S_p^0} \right) + \frac{i\pi}{S_0^0} e^{-i\nu \omega_p} \right\}, \quad (54)$$

where we used Eq. (51) for the integral over $k\bar{\rho}$ and defined $\omega_p = \pi S_p^0/S_0^0$. Since all the quantities on the right-hand side of Eq. (54) are known, this formula provides an explicit rep-

resentation of the roots k_n of the spectral Eq. (29) in terms of the geometric characteristics and the classical properties of the graph.

In Ref. [18] a mathematical proof is presented, which assures us that Eq. (54) converges. In addition it is proved in Ref. [18] that Eq. (54) converges to the exact spectral eigenvalues. Both convergence, and convergence to the correct results are illustrated with the help of a specific example in Sec. IV. It is also proved in Ref. [18] that the series (54) may only be conditionally convergent. This means that for proper convergence the ordering of the terms in Eq. (54) is important. Proper convergence of Eq. (54) is obtained if the terms in Eq. (54) are ordered according to the code lengths of the periodic orbits [18]. In other words, the sum in Eq. (54) is to be extended over all periodic orbits with code lengths smaller than or equal to l , which yields the approximation $k_n(l)$ to k_n . Then, on the basis of the results obtained in Ref. [18], we have $\lim_{l \rightarrow \infty} k_n(l) = k_n$. This means that Eq. (54) is exact. It is important to note here that the ordering of terms in Eq. (54) is *not* according to their action lengths, but according to the lengths of the code words that code for the periodic orbits. This is intuitively understandable, since the code length l is connected to the power n of the S matrix in Eq. (33) according to $l = n/2$.

The expansion (54) provides an explicit representation of the roots of the spectral equation (29) in terms of the geometric characteristics of the graph. In a similar way one can obtain explicit expansions for any power of the energy levels k_n^m or any function of the eigenvalues $f(k_n)$.

IV. EXAMPLES

The coefficients A_p in Eq. (54) assume a particularly simple form in the case of linear graphs with $\lambda_i^0 = 0$, $i = 1, \dots, N_V$. Both the vertices and the bonds of a linear graph can be naturally labeled by means of a single index such that $B_{1,2} \equiv B_1$, $B_{2,3} \equiv B_2$, \dots , $B_{N_V-1, N_V} \equiv B_{N_V-1}$ (see Fig. 2). The scaling coefficients for the momentum of the particle are correspondingly $\beta_{1,2} \equiv \beta_1$, $\beta_{2,3} \equiv \beta_2$, \dots , $\beta_{N_V-1, N_V} \equiv \beta_{N_V-1}$, the bond lengths are $L_{1,2} \equiv L_1$, $L_{2,3} \equiv L_2$, \dots , $L_{N_V-1, N_V} \equiv L_{N_V-1}$, the potentials are $U_{1,2} \equiv U_1$, $U_{2,3} \equiv U_2$, \dots , $U_{N_V-1, N_V} \equiv U_{N_V-1}$ and the reduced bond actions are $S_{1,2}^0 \equiv S_1^0 = \beta_1 L_1$, $S_{2,3}^0 \equiv S_2^0 = \beta_2 L_2$, \dots , $S_{N_V-1, N_V}^0 \equiv S_{N_V-1}^0 = \beta_{N_V-1} L_{N_V-1}$, respectively. In this case, if a prime periodic orbit p undergoes σ_p^i reflections from a vertex V_i and $2\tau_p^i$ transmissions through it, the weight coefficient in the expansion (39) is [17]

$$A_p = \prod_i r_i^{\sigma_p^i} (1 - r_i^2)^{\tau_p^i}, \quad (55)$$

where r_i is the reflection coefficient from the vertex V_i , and the product is taken over all the vertices encountered by the orbit p . If a particle reflects from the vertex V_i traveling along the bond B_i , the reflection coefficient is

TABLE I. Successive approximations of the eigenvalues k_1 (first row), k_{10} (second row), and k_{100} (third row) of a specific scaling step potential (see text for details) as a function of the code length l (columns 2–5). The exact values of k_1 , k_{10} , and k_{100} are listed in column 6. Column 7 lists the absolute errors $|k_n(l=20) - k_n|$ for $n=1, 10$, and 100 .

Root	$l=5$	$l=10$	$l=15$	$l=20$	Exact	Error
k_1	4.11608	4.11653	4.10721	4.10513	4.10715	0.00202
k_{10}	39.28658	39.29807	39.30730	39.30521	39.30521	0.00000
k_{100}	394.94770	394.95647	394.96622	394.96456	394.96471	0.00016

$$r_i = \frac{\beta_{i-1} - \beta_i}{\beta_{i-1} + \beta_i}, \quad i=2, \dots, N_V-1, \quad r_1 = -1, \quad r_{N_V} = -1. \quad (56)$$

We assumed Dirichlet boundary conditions at the left and right dead ends of the graph. The reflection coefficient changes its sign if the reflection happens from the side of the bond B_{i+1} . If, for a given orbit, the total number of reflections with $r_i < 0$ is χ_p , then

$$A_p = (-1)^{\chi_p} \prod_i |r_i|^{\sigma_p^i} (1 - r_i^2)^{\tau_p^i}. \quad (57)$$

The two-vertex linear graph is trivial and corresponds to a quantum particle in a square-well box. A quantum particle moving in a scaling step potential as shown in Fig. 3, gives rise to the simplest nontrivial graph, the scaling three-vertex linear graph, shown on the bottom of Fig. 3. In this case there is only one nontrivial reflection coefficient

$$r_2 = \frac{\beta_1 - \beta_2}{\beta_1 + \beta_2}. \quad (58)$$

All the periodic orbits of the three-vertex linear graph shown in Fig. 3 correspond one to one with words formed from a binary code with two letters \mathcal{L} and \mathcal{R} [17–19], where \mathcal{L} stands for a reflection of the orbit off the leftmost vertex (left-hand potential wall), and \mathcal{R} stands for a reflection off the rightmost vertex (right-hand wall). Thus the \mathcal{L} , \mathcal{R} code is unique and complete. For this system the spectral equation is

$$\sin(S_0^0 k) - r_2 \sin(\Omega_1 k) = 0, \quad (59)$$

where $S_0^0 = S_1^0 + S_2^0$ is the total reduced action of the graph and $\Omega_1 = S_1^0 - S_2^0$. With $a_1 = r_2$ and $\gamma_0 = \gamma_1 = \pi/2$, Eq. (59) is of the form (44), (45) and the number of cos terms in $\phi(k)$ (in this case one term) complies with the estimate (46). Because of $|r_2| < 1$, it is the spectral equation of a regular quantum graph. Using the explicit form (57) of the coefficients A_p in the expansion (54), we obtain the explicit series expansion for every root k_n of Eq. (59). Thus the spectrum of the scaling step potential shown in Fig. 3 may be calculated explicitly and analytically with the help of Eq. (54). This by itself is a considerable advance in the theory of simple one-dimensional quantum systems, which up to now could only be solved using graphical or numerical techniques [14,20,21].

We illustrate the method and the convergence of the series expansion (54) with the following concrete, dimensioned example of the scaling step potential of Fig. 3. Choosing $b = 0.3$, $\lambda_1 = 0$, and $\lambda_2 = 1/2$, we computed the solutions k_1 , k_{10} , and k_{100} of Eq. (59) using three different methods: (i) exact numerical, (ii) explicit periodic-orbit expansion (54) of the individual eigenvalues and (iii) numerical integration using the S -matrix representation (33) of the density of states. Addressing (i) we obtained the exact numerical values of the three selected roots of Eq. (59). The result is $k_1 = 4.107149$, $k_{10} = 39.305209$, and $k_{100} = 394.964713$.

Turning to method (ii) we recomputed these three eigenvalues using Eq. (54) directly including progressively more periodic orbits in the expansion (54). The result is presented in Table I that shows the values of k_1 , k_{10} and k_{100} computed with Eq. (54) including periodic orbits coded by binary words of length $l=5, 10, 15$, and 20 , respectively. This corresponds to including 23, 261, 4807, and 111 321 periodic orbits in the expansion (54), respectively. We observe that the accuracy does not improve monotonically, but that there is a definite overall improvement of accuracy with the code length. As a matter of fact, as discussed above and shown mathematically in [18], the series (54) converges, and converges to the exact results of k_n in the limit of $l \rightarrow \infty$.

Turning to method (iii) we note that due to the exponential proliferation of periodic orbits, it becomes progressively more difficult to compute the codes of longer periodic orbits. Nevertheless, with the help of a numerical procedure, we are able to illustrate the convergence behavior of Eq. (54) for code lengths much longer than $l=20$. Starting from Eq. (33) we compute the S matrix numerically and perform all the steps leading up to Eq. (54) numerically. In particular, this method involves numerical computation of S -matrix powers and numerical integration over k . Within any given level of numerical accuracy this method is completely equivalent to the method of summing the orbits, but allows us to extend the computations such that we effectively include all periodic orbits up to code length $l=150$. This corresponds roughly to $2^{150} = 1.4 \times 10^{45}$ periodic orbits, since the periodic orbits on the three-vertex linear graph are coded by a binary code. This estimate is substantiated by an analytical estimate of the number of periodic orbits. For the three-vertex graph the periodic orbits are binary necklaces over the two symbols \mathcal{L} and \mathcal{R} [18]. The number of binary necklaces of length ℓ is given by [22]

$$\mathcal{N}(\ell) = \frac{1}{\ell} \sum_{n|\ell} \phi(n) 2^{\ell/n}, \quad (60)$$

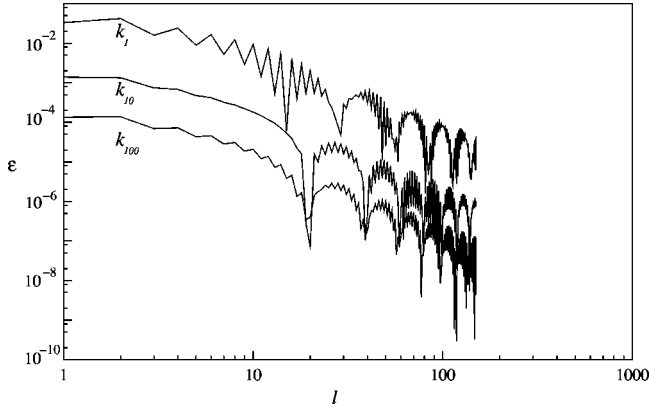


FIG. 4. The deviation $\epsilon_l = |k_n(l) - k_n|/k_n$ of the exact eigenvalues for k_1 , k_{10} , and k_{100} from the corresponding values obtained via the series representation, as a function of the lengths l of the periodic orbits.

where the symbol “ $n|\ell$ ” denotes “ n is a divisor of ℓ ,” and $\phi(n)$ is Euler’s totient function defined as the number of positive integers smaller than n and relatively prime to n with $\phi(1) = 1$ as a useful convention. An upper limit for Λ is obtained if we use Eq. (60) in the case where ℓ is a prime number. In this case (60) reduces to

$$\mathcal{N}(p) = \frac{1}{p} [\phi(1)2^p + \phi(p)2^1] = \frac{1}{p} [2^p + 2(p-1)], \quad (61)$$

where p is prime. Thus, in the limit of $p \rightarrow \infty$ we have $\mathcal{N}(p) \rightarrow 2^p/p$, and therefore,

$$\Lambda = \lim_{p \rightarrow \infty} \frac{\ln[\mathcal{N}(p)]}{p} = \ln(2). \quad (62)$$

Thus, according to this estimate, the total number of periodic orbits of length 150 is again

$$\mathcal{N}(150) \sim e^{150\Lambda} = 2^{150}. \quad (63)$$

We also computed numerical estimates of Λ . Using the exact formula (60) for counting periodic orbits in Eq. (34) and including periodic orbits with code lengths of up to $l = 1000$, we found $\Lambda > 1.987$, consistent with the estimate (62). For $l = 150$, relevant for our numerical example, the asymptotic regime is not yet reached and we find $\Lambda \approx \ln(1.943)$. This value for Λ can be used for a more refined estimate of the number of periodic orbits of length $l = 150$, $\mathcal{N}(150) \approx 1.943^{150} \approx 2 \times 10^{43}$. Clearly, computing the codes of that many periodic orbits and summing them up in Eq. (54) is beyond the storage capacity and power of any currently existing computer, but is apparently no obstacle to the numerical simulation of that many periodic orbits included in Eq. (54). Figure 4 illustrates the rate of convergence of the eigenvalues k_1 , k_{10} , and k_{100} obtained with method (iii) as a function of code length $l \leq 150$. Shown is the relative error $\epsilon_l = |k_n(l) - k_n|/k_n$ for $n = 1, 10$, and 100 .

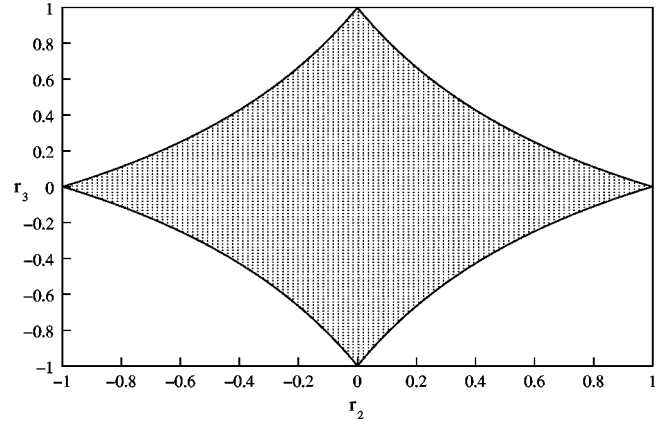


FIG. 5. Parameter space (r_2, r_3) of a four-vertex linear quantum graph. Parameter combinations in the shaded region correspond to regular quantum graphs. This demonstrates that the subset of regular quantum graphs within the set of all four-vertex linear quantum graphs is nonempty and in fact of finite measure.

The error is seen to decrease on average as a function of the increasing periodic-orbit length l . From Fig. 4 we obtain approximately $\epsilon_l = |k_n(l) - k_n|/k_n \sim 1/l^2$ on average.

For a four-vertex linear graph, the spectral equation is

$$\sin(S_0^0 k) = r_3 \sin(\Omega_1 k) - r_2 r_3 \sin(\Omega_2 k) + r_2 \sin(\Omega_3 k), \quad (64)$$

where $S_0^0 = S_1^0 + S_2^0 + S_3^0$, $\Omega_1 = S_1^0 + S_2^0 - S_3^0$, $\Omega_2 = S_1^0 - S_2^0 + S_3^0$, $\Omega_3 = S_1^0 - S_2^0 - S_3^0$ and r_2, r_3 are the reflection coefficients at the vertices V_2 and V_3 , respectively. With $\gamma_i = \pi/2$, $i = 0, 1, 2, 3$, this spectral equation is of the form (44), (45) and the number of cos terms in $\phi(k)$ (three in this case) complies with Eq. (46). For

$$|r_3| + |r_2 r_3| + |r_2| < 1 \quad (65)$$

the four-vertex linear graph is regular. In this case the energy values of the four-vertex linear graph may be calculated exactly using the periodic-orbit expansion (54). According to Fig. 5 the set of r_2, r_3 values that fulfill Eq. (65) occupies a diamond-shaped area bounded by the functions $r_3 = \pm(1 - |r_2|)/(1 + |r_2|)$. This observation proves that regular quantum graphs are an important, finite-measure subset of quantum graphs.

The set of regular quantum graphs is much wider than the three- and four-vertex quantum graphs discussed in detail above. Since, as indicated by Eqs. (59) and (64), the amplitudes a_i in Eq. (45) involve products of vertex reflection coefficients, and since the vertex reflection coefficients of a linear quantum graph (via proper choice of the bond potentials) are free parameters of the quantum graph, a finite-measure set of regular quantum graphs exists for *any* given linear graph. It is possible that more complex graph topologies, such as, rings and stars, may also admit a set of regular quantum graphs. This topic is currently under investigation.

V. DISCUSSION, SUMMARY, AND CONCLUSION

In this paper we defined and studied a subset of quantum graphs: regular quantum graphs. Regular quantum graphs satisfy the regularity condition (47), which implies that the roots of the spectral equation are confined to regularly spaced root intervals. One and only one root is found per root interval. This property allows us to derive rigorous, converging periodic-orbit expansions for individual energy levels of regular quantum graphs.

We often hear the comment that the expansion (54) for k_n cannot possibly converge, since Eq. (39) is divergent. This comment is invalid. There is a fundamental difference between Eq. (39) and Eq. (54). Equation (39) is a periodic-orbit expansion of the kernel of a functional (a series of Dirac δ “functions”), whereas Eq. (54) is a periodic-orbit expansion of a simple c number. On the level of Eq. (39) the concepts of convergence or divergence are not even defined. Only after multiplying Eq. (39) with a test function [23] and integrating over k , are the concepts of divergence and convergence defined. In this sense even Eq. (39) is convergent. This is also known as convergence in the distribution sense [23] and leads to proper convergence in the usual sense of elementary undergraduate-level analysis. Thus, the convergence of Eq. (54) is no longer a mystery.

Another more serious comment concerns the sense in which quantum graphs are classically chaotic. Quantum graphs are based on a one-dimensional network of vertices and bonds. Therefore, a dynamical Liapunov exponent [1,24] cannot be defined in the traditional sense of exponentially diverging initially close trajectories. As explained in [3], however, this is no obstacle to associate a classical phase space with a quantum graph and to show that the classical dynamics in this phase space is mixing [3]. Moreover, quantum graphs fulfill another property of quantum chaos, the exponential proliferation of classical periodic orbits as manifested by a positive topological entropy (see Secs. III and IV). Therefore, quantum graphs have been called “paradigms of quantum chaos” [7]. Inasmuch as the positive topological entropy is concerned, regular quantum graphs qualify as quantum chaotic systems. Regular quantum graphs do not show all the characteristics of “fully developed” quantum chaos. For instance, due to the existence of the forbidden zones R_n (see Sec. III) they definitely do not show a Wignerian nearest neighbor statistics. We do not believe that this is a problem, since there is no universally accepted rigorous definition of quantum chaos that requires “Wignerian statistics” as one of the necessary conditions. The only broadly accepted criterion is that “quantum chaos” deals with quantum systems that are chaotic in their classical limit. Based on this criterion, together with the mixing property [3] and the positive topological entropy (see Sec. IV), regular

quantum graphs definitely qualify as quantum chaotic systems, i.e., systems chaotic in the classical limit.

A more delicate point concerns the derivation of Eq. (54) by integrating the fluctuating part in Eq. (39) term by term. Since the resulting periodic-orbit expansion may only be conditionally convergent, this is reason for concern. We addressed this point from a rigorous mathematical point of view in [18]. We were able to prove rigorously that the interchange of integration and summation in the k integral of $k\rho(k)$ is allowed. Thus, term-by-term integration of Eq. (39) is justified, validating the final result (54).

To our knowledge this is the first time that the energy levels of a class of classically chaotic systems are expressed one by one with the help of convergent periodic-orbit expansions. Studying specific examples of regular quantum graphs we proved that the class of regular quantum graphs is not empty; it is in fact an important finite-measure subset of quantum graphs. The explicit formulas of individual quantum energy levels obtained in this paper remind us of the Einstein-Brillouin-Keller (EBK) method [1] for the quantization of integrable classical systems. But there are important differences. Regular quantum graphs do not correspond to classically integrable systems. In fact, due to the importance of non-Newtonian periodic orbits, the number of classical periodic orbits proliferates exponentially with the code length. This proves that even regular quantum graphs, as defined by the regularity condition (47), are classically chaotic systems with a positive topological entropy. For one of our examples, the scaling step potential discussed in Sec. IV, we computed estimates of the topological entropy analytically and numerically. In both cases it turned out to be positive and close to $\ln(2)$. This proves that, at least for the cases studied, the classical limit is chaotic. Another difference to EBK theory is that the periodic orbits in regular quantum graphs are not confined to phase-space tori. Finally, in contrast with EBK theory—a semiclassical theory that does not usually return exact results—our formulas are mathematically exact. In summary, despite the apparent complexity and exponential proliferation of the periodic orbits of regular quantum graphs, the organization of the roots of the spectral equation into regularly spaced intervals makes it possible to pinpoint every single energy eigenvalue of a regular quantum graph analytically and exactly by an explicit, convergent periodic-orbit expansion.

ACKNOWLEDGMENTS

Y.D. and R.B. gratefully acknowledge financial support by NSF Grant Nos. PHY-9900730 and PHY-9984075; Y.D. and R.V.J. were supported by NSF Grant No. PHY-9900746.

-
- [1] M. Gutzwiller, *Chaos in Classical and Quantum Mechanics* (Springer, New York, 1990).
 [2] Yu. Dabaghian, R. V. Jensen, and R. Blümel, Pis'ma Zh. Éksp. Teor. Fiz. **74**, 258 (2001) [JETP Lett. **74**, 235 (2001)].

- [3] T. Kottos and U. Smilansky, Phys. Rev. Lett. **79**, 4794 (1997); Ann. Phys. (N.Y.) **274**, 76 (1999).
 [4] E. Akkermans, A. Comtet, J. Desbois, G. Montambaux, and C. Texier, e-print cond-mat/9911183.

- [5] M. Pascaud and G. Montambaux, Phys. Rev. Lett. **82**, 4512 (1999).
- [6] F. Barra and P. Gaspard, Phys. Rev. E **63**, 066215 (2001).
- [7] U. Smilansky, J. Phys. A **33**, 2299 (2000).
- [8] O. Bohigas, M.-J. Giannoni, and C. Schmit, Phys. Rev. Lett. **52**, 1 (1984).
- [9] *Chaos et Physique Quantique—Chaos and Quantum Physics*, Proceedings of the Les Houches Summer School, Session LII, edited by M.-J. Giannoni, A. Voros, and J. Zinn-Justin (Elsevier Science, Amsterdam, 1991).
- [10] L. Couchman, E. Ott, and T. M. Antonsen, Jr., Phys. Rev. A **46**, 6193 (1992).
- [11] R. E. Prange, E. Ott, T. M. Antonsen, B. Georgeot, and R. Blümel, Phys. Rev. E **53**, 207 (1996).
- [12] R. Blümel, T. M. Antonsen, Jr., B. Georgeot, E. Ott, and R. E. Prange, Phys. Rev. E **76**, 2476 (1996); **53**, 3284 (1996).
- [13] I. M. Lifshits, S. A. Gredeskul, and L. A. Pastur, *Introduction to the Theory of Disordered Systems* (Wiley Interscience, New York, 1988).
- [14] L. D. Landau and E. M. Lifshitz, *Quantum Mechanics* (Pergamon, Oxford, 1960).
- [15] L. Sirko, P. M. Koch, and R. Blümel, Phys. Rev. Lett. **78**, 2940 (1997).
- [16] Sz. Bauch, A. Błędowski, L. Sirko, P. M. Koch, and R. Blümel, Phys. Rev. E **57**, 304 (1998).
- [17] Y. Dabaghian, R. V. Jensen, and R. Blümel, Phys. Rev. E **63**, 066201 (2001).
- [18] R. Blümel, Yu. Dabaghian, and R. V. Jensen (unpublished).
- [19] R. Blümel and Yu. Dabaghian, J. Math. Phys. **42**, 5832 (2001).
- [20] S. Flügge, *Practical Quantum Mechanics I* (Springer, New York, 1971), Problem 26.
- [21] L. I. Schiff, *Quantum Mechanics* (McGraw-Hill, New York, 1955).
- [22] J. Riordan, *An Introduction to Combinatorial Analysis* (Wiley, New York, 1958).
- [23] W. Walter, *Einführung in die Theorie der Distributionen* (Bibliographisches Institut, Mannheim, Germany, 1974).
- [24] E. Ott, *Chaos in Dynamical Systems* (Cambridge University Press, Cambridge, 1993).